Orientational disorder in adamantane and adamantanecarboxylic acid

E. O. R. Beake[1] M. G. Tucker[2,3] M. T. Dove[1,*] A. E. Phillips[1,*]

[1]School of Physics and Astronomy, Queen Mary University of London, Mile End Road, London E1 4NS, U.K.
[2]ISIS Neutron and Muon Source, Rutherford Appleton Laboratory, Harwell Oxford, Didcot OX11 0QX, U.K.
[3]Spallation Neutron Source, Oak Ridge National Laboratory, Oak Ridge, TN 37830, U.S.A. (current address)
a.e.phillips@qmul.ac.uk, martin.dove@qmul.ac.uk

Abstract The molecular crystals adamantane, $C_{10}H_{16}$, and adamantanecarboxylic acid, $C_{10}H_{15}COOH$, undergo order-disorder phase transitions at 208 and 250 K respectively. Reverse Monte Carlo refinement of total neutron scattering data collected from deuterated samples immediately above these phase transitions shows that the high-temperature phases are well described by models in which the adamantyl groups are disordered over two sites. No correlation between the orientations of neighbouring molecules is observed. These results demonstrate that the intermolecular potential energy of these materials depends strongly on the orientation of the reference molecule but only very weakly on the orientations of its neighbours.

The diamondoids are a class of hydrocarbons in which a small section of the diamond structure is capped with hydrogen atoms at the surface. Occuring naturally in, and isolatable from, natural oil and gas,[1] they are readily functionalisable and useful as synthetic chemistry building blocks,[1] while their negative electron affinity[2] gives rise to applications as high-brilliance, femtosecond-pulse electron emitters.[3] Although, like other small molecules, they can be isolated and purified in chemically well defined compositions, they also resemble nanoparticles in that the chemical and physical environment of their core and surface are substantially different. This structure allows each carbon atom within a molecule to have an ideal tetrahedral bonding geometry, producing highly stable molecules. The interactions between these molecules, on the other hand, are dominated by van der Waals forces between hydrogen atoms. Although these forces are traditionally labelled "weak", in fact they are surprisingly strong and play an important role in stabilising crystal structures.[4] More dramatically, the strength of hydrogen-hydrogen dispersion forces is demonstrated by their capacity to stretch stable covalent carbon-carbon bonds far beyond their usual equilibrium length.[5] The assembly of diamondoid molecules into solids is thus directed by the strong intermolecular hydrogen-hydrogen interactions, which also play an important role in these materials' physical properties including plasticity, polymorphism, and gel formation.[6]

	T, K	ΔH, kJ mol^{-1}	ΔS, J K^{-1} mol^{-1}	ref.
$C_{10}H_{16}$	208	3.38	16.2	[7]
$C_{10}H_{15}COOH$	251	2.25	8.97	[8]

Table 1: Thermodynamic parameters of the phase transitions of adamantane and adamantanecarboxylic acid.

We here consider the order-disorder phase transitions in adamantane, $C_{10}H_{16}$, and adamantanecarboxylic acid, $C_{10}H_{15}COOH$. Adamantane itself is the simplest of the diamondoid molecules and is almost spherical, able to rotate in three dimensions without obvious steric hindrance; adamantanecarboxylic acid crystallises as a typical carboxylic acid dimer, forming an elongated cylinder shape that is able to rotate about a single axis. Both materials crystallise in a dynamically disordered phase at room temperature but freeze into an ordered configuration on cooling (Table 1). Similar phase transitions are known for many other adamantane derivatives.[9–12] These phase transitions provide an opportunity to study the energy landscapes associated with the orientational degrees of freedom. While some information about orientational disorder can be inferred from calorimetric measurements, there are many other contributions to the entropy of transition, so that it is not straightforward to determine orientational disorder from calorimetry alone.[9,13] On the other hand, the reported crystal structures of the disordered phases are necessarily spatial averages that do not take into account any local correlations between the orientations of adjacent molecules. We here report a study of these materials using total neutron scattering, a method that overcomes both of these disadvantages by measuring both the Bragg and diffuse scattering, in order to model both the crystalline order and local deviations from the crystallographic symmetry of the disordered phases.

As a result of its very high molecular symmetry, adamantane crystallises in a disordered face-centred cubic structure

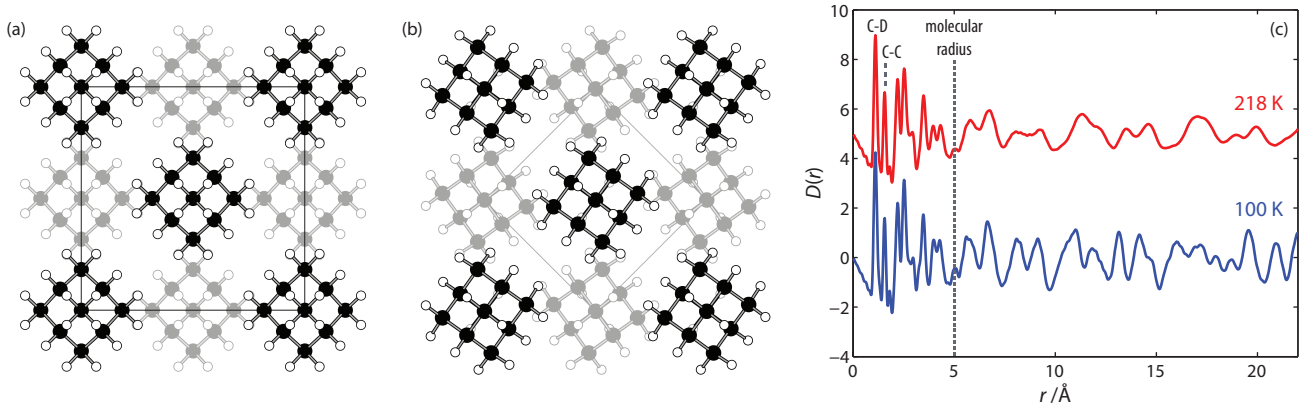

Figure 1: Structure of adamantane in (a) the high-temperature and (b) the low-temperature phase, and (c) the experimental pair distribution functions in both phases.

at room temperature ($Fm\bar{3}m$, $a = 9.426$ Å, $Z = 4$); it transforms to a tetragonal phase at 208 K ($P\bar{4}2_1c$, $a = 6.614$ Å, $c = 8.875$ Å, $Z = 2$).[14,15] As one might expect from a phase transition associated with a significant decrease in volume, this can also be induced by increased pressure.[16–19] The disorder in the high-temperature phase arises from the fact that the centroid of each molecule is a crystallographic centre of symmetry although the molecules themselves are not centrosymmetric. The relationship between the two orientations at each site can equally be described as a fourfold rotation or mirror plane. Jumps between these two orientations occur by fourfold rotation and have been observed by NMR[20] and quasielastic neutron scattering.[21]

This phase transition is unusual in that $P\bar{4}2_1c$ is not an isotropy subgroup of $Fm\bar{3}m$, implying that at least two coupled primary order parameters are needed to describe the transition.[22,23] In the ordered phase, planes of molecules alternate between the two high-temperature orientations; in addition, though, the same planes alternate in the direction of a rotation of about 9° about the c-axis. Thus this is both an order-disorder phase transition with respect to the first of these order parameters and a displacive transition with respect to the second. The first effect alone would correspond to the X_2^- irrep and a low-temperature space group of $P4_2/nmc$; the second would correspond to the X_3^+ irrep and a space group of $P4/mnc$. A similar case of coupled order parameters describing molecular rotations occurs in $(NH_4)_2MgF_4$, where a first-order phase transition on cooling involves rotation of the ammonium ions in two distinct senses.[24]

By contrast, adamantanecarboxylic acid in both its high- and low-temperature phases has a triclinic unit cell, space group $P\bar{1}$, with two molecules per unit cell that exist as a dimer, shown in figure 2. The low-temperature phase ($a = 6.452(3)$ Å, $b = 6.681(2)$ Å, $c = 11.510(3)$ Å, $\alpha = 80.84(2)°$, $\beta = 87.22(3)°$, $\gamma = 74.11(3)°$) is ordered while above the phase transition at 251 K the high-temperature phase ($a = 6.503(2)$ Å, $b = 6.849(2)$ Å, $c = 11.620(4)$ Å, $\alpha = 77.11(2)°$, $\beta = 85.77(2)°$, $\gamma = 76.34(2)°$) is disordered. In the high-temperature phase the adamantyl groups of different dimers occupy two orientations, in an approximate 40:60 proportion, staggered with respect to one another, while the two carboxylate groups have similar orientations. The hydrogen bonds between carboxylic acid groups prevent rotation of the adamantanecarboxylic acid dimer about the two axes perpendicular to the molecular axis,[25] thus restricting rotation such that the dimer can only rotate about its own axis.

Neutron total scattering data were collected at various temperatures on the POLARIS diffractometer at the ISIS spallation neutron facility. Powder samples of perdeuterated adamantane and adamantanecarboxylic acid, deuterated except at the acid proton (both as purchased from QMX), were contained within a thin-walled vanadium can of diameter 8 mm, which was held in a He exchange gas cryostat. Measurements were also performed on the backgrounds from the empty instrument and the empty can within the cryostat, and of a vanadium rod for normalisation. The background was subtracted, the data normalised using standard methods, and a Fourier transform performed on the normalised total scattering data to calculate the pair distribution function, using the program Gudrun.[26] Separately, Le Bail fits were performed using the EXPGUI[27] interface to GSAS[28] in order to extract background and peak shape parameters for subsequent fitting.

Thus for each material at each temperature studied three functions were extracted from the raw data: the pair distribution function (PDF) $D(r)$, the scattering function $i(Q)$, and the diffraction profile from a single diffractometer bank, expressed for the time-of-flight instrument as $I(t)$. An atomic configuration within a supercell of side length approximately 50 Å was fit to these three data sets using the reverse Monte Carlo (RMC) algorithm as implemented in the program RMCProfile.[29] This approach differs from other RMC algorithms

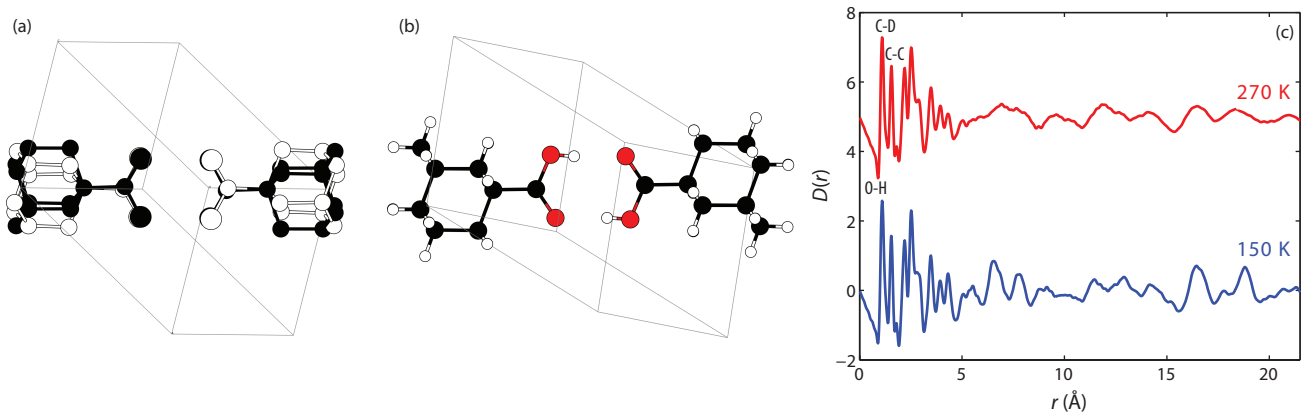

Figure 2: (a) Structure of adamantanecarboxylic acid in the high-temperature phase. The two orientations of each molecule are shown in black and white. Carbon atoms are small circles, oxygen atoms large circles; for clarity hydrogen atoms are not shown. (b) Structure of the same material in the low-temperature phase. Here carbons are shown in black, hydrogens in white, oxygens in red. (c) The experimental pair distribution functions in both phases. There is a noticable sharpening in the ordered phase in the region around 7 Å, corresponding to correlations between the orientations of molecules in the same dimer. Note the small negative peak at 1 Å, corresponding to the O−^{1}H bond.

such as RMC-POT[30] and hybrid RMC,[31] which are designed for amorphous systems and therefore do not refine against the diffraction profile. Although it is difficult to ensure complete consistency between the Bragg scattering and PDF, a point we discuss in detail below, this approach is necessary to maintain an appropriate degree of crystallinity while using a relatively small simulated supercell.

The initial configurations were produced based on lattice parameters from the Le Bail refinement, with a $5 \times 5 \times 5$ supercell (13 000 atoms) for adamantane and a $7 \times 7 \times 4$ supercell (11 368 atoms) for adamantanecarboxylic acid. Each adamantane molecule was initially randomly rotated about all three axes, so that the orientations were uniformly distributed on a spherical surface (Fig. 3(a)); similarly, each adamantanecarboxylic acid dimer was initially randomly rotated about its long axis, giving orientations uniformly distributed on a circle (Fig. 3(c)). In order to discourage chemically implausible configurations, potentials based on the MM3 data set[32] were applied to both materials, restraining the C−C and C−D bonds and C−C−C and C−C−D angles. In addition, in adamantanecarboxylic acid, the C−O and O−H bonds and O−C−O, C−C−O, and C−O−H angles were restrained, and the ten atoms of the carboxylic acid dimer and bonded adamantyl carbon $(CCOOH)_2$ were restrained to lie in a plane. Our use of intramolecular potentials also differs subtly from the other approaches listed above, in that we are simply aiming to maintain the known molecular shapes, rather than directing the simulation towards geometries not originally present. This method discourages the simulation from accessing obviously unphysical regions of parameter-space while maintaining a direct connection between the simulation and the experimental data: the final results are independent of small changes in the Hamiltonian used. Each individual RMC step consisted of moving a random atom by a random distance up to a predetermined limit, accepting or rejecting the move according to the Metropolis algorithm.

During the RMC refinements of both materials it was found that the total chi-squared decreased towards a converged minimum value after approximately 10^7 atomic moves, or over 750 moves per atom. For each data set, six independent RMC refinements were performed to give improved statistical accuracy to extracted histograms, averages and standard deviations. Examples of the final fits to the three functions are shown in Fig. 4 and sample refined configurations are provided as Supporting Information. Although small, the residuals from this refinement are larger than would be achieved from refinement of any one data set alone. This suggests that there may be slight inconsistencies between the different data sets for each material. In particular, the PDF and Bragg data sets indicate slightly different Debye-Waller factors.

This minor inconsistency is likely to have arisen in the following way. On the one hand, during Rietveld refinement, the diffraction intensity at low t (high d-spacing), where many peaks overlap, cannot be unambiguously divided between these peaks and the background. As a result, there is substantial correlation between the atomic displacement parameters and the background. Since, in our method, the background function is imported into RMC refinement directly from the Rietveld fit and is not refined any further, if the background at low t is slightly too low, achieving a perfect fit to the Bragg data in the RMC refinement will require a configuration with slightly *smaller* mean-square atomic displacements than the real sample. On the other hand, the measured PDF is necessarily broadened slightly since it is calculated by taking the Fourier transform of data measured over a finite Q range. One of the advantages of neutron

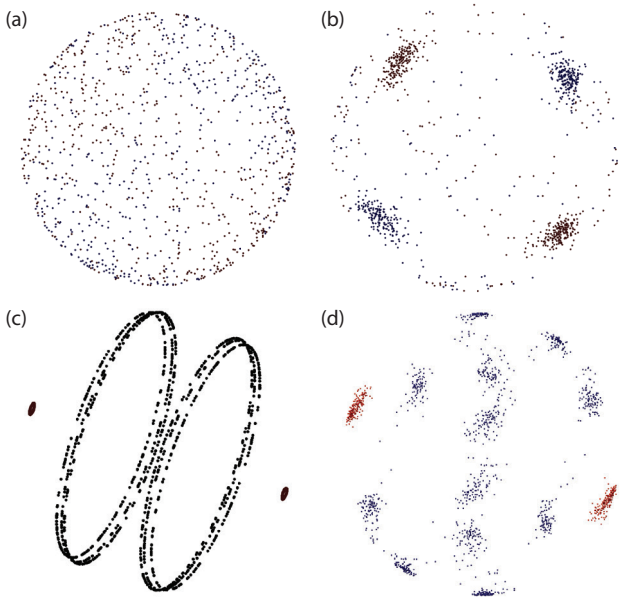

Figure 3: Stereographic projections of the molecular orientations in the disordered phases of the two compounds, as determined by RMC modelling. Only the four methine carbons are shown. Adamantane: (a) in the initial configuration, (b) after refinement; the two orientations are shown in blue and red. Adamantanecarboxylic acid: (c) in the initial configuration, (d) after refinement. The carbon atom bonded to the COOH moeity is shown in red.

Adamantane, 218 K	
C–D, Å	1.10(7)
C–C, Å	1.50(6)
∠C–C–D, °	110(7)
∠C–C–C, °	109(4)
∠ tetrahedral, °	109.5(17)
Adamantanecarboxylic acid, 270 K	
C–D, Å	1.10(8)
C–C, Å	1.53(6)
C–O, Å	1.36(25)
C=O, Å	1.24(27)
O–H, Å	1.10(35)
∠C–C–D, °	110(6)
∠C–C–C, °	109(5)
∠O–C=O, °	120(3)
∠ tetrahedral, °	110(3)
ω, 10^{-4} Å^2	19(11)

Table 2: Intramolecular geometric parameters for the refined configurations of both molecules, averaged over every molecule in six independent simulation cells. Uncertainties shown are the sample standard deviations. The "tetrahedral" angle is between two methine carbons and the centre of mass of the molecule or adamantyl group. The deviation from planarity ω is the sum of the squared deviations of the $(COOH)_2$ atoms from the best-fit plane.

radiation for total scattering measurements is that the ability to measure to very high Q, which minimises this effect; nonetheless, achieving a perfect fit to the PDF data in the RMC refinement will require a configuration with slightly *greater* mean-square atomic displacements than the real sample. Although we have endeavoured to minimise both these effects, their combination may make it impossible to achieve a perfect fit to the PDF and Bragg data simultaneously, with the precise final RMC-refined configuration depending on the relative weights assigned to the two data sets in the chi-squared function. Crucially, however, the results we present below are not sensitive to small changes in the RMC weight of the two data sets or to details of how they are prepared (e.g., the maximum Q over which the Fourier transform is taken or the background of the Bragg data set).

The intramolecular potentials successfully maintained the molecular geometries during RMC refinement (Table 2). The final orientations of the molecules are shown in Fig. 3 (b) and (d). In both materials, the orientation distributions in the high-temperature phase cluster about the average disordered structure known from conventional structure refinement. We searched these distributions for evidence of local ordering, assigning each molecule to one of the two possible disordered orientations to create an Ising model representation of the system. In adamantane, this procedure meant we considered only the X_2^- order parameter, corresponding to inversion; the X_3^+ order parameter, corresponding to the 9° rotation, was too subtle to be resolved. For the close-packed adamantane structure, each molecule is clearly surrounded by 12 nearest neighbours. In adamantanecarboxylic acid, adamantyl groups are packed in bilayers parallel to the *ab* plane. We considered two such groups to be nearest neighbours if their centroids, in the low-temperature phase, were less than 7 Å apart; thus each adamantyl has seven nearest neighbours: four in its own layer and three in the adjacent layer.

For each material we considered two measures of local order. First, for each adamantyl group we counted the number of nearest neighbours n in the correct (ordered) orientation with respect to the original group. In the ordered phase of adamantane, four of each molecule's nearest neighbours, in a plane, have the same orientation as the central molecule, while the remaining eight have the opposite orientation. In the ordered phase of adamantanecarboxylic acid, the four neighbours in the same layer as the original adamantyl group have the same orientation, while the three in the neighbouring plane have the opposite. Thus for adamantane, the possible values of n run from 0 to 12; for adamantanecarboxylic acid, they run from 0 to 7. For adamantane, an n value can be assigned in three possible ways corresponding to the three possible unique (tetragonal z) axes; in our calculation the maximum such score was chosen for each molecule.

The second measure of local order we considered is the "orientational correlation function" defined in a previous MD study[33] by $O_i = \sum_{j=1}^{N} s_i s_j$, where j runs over the N nearest

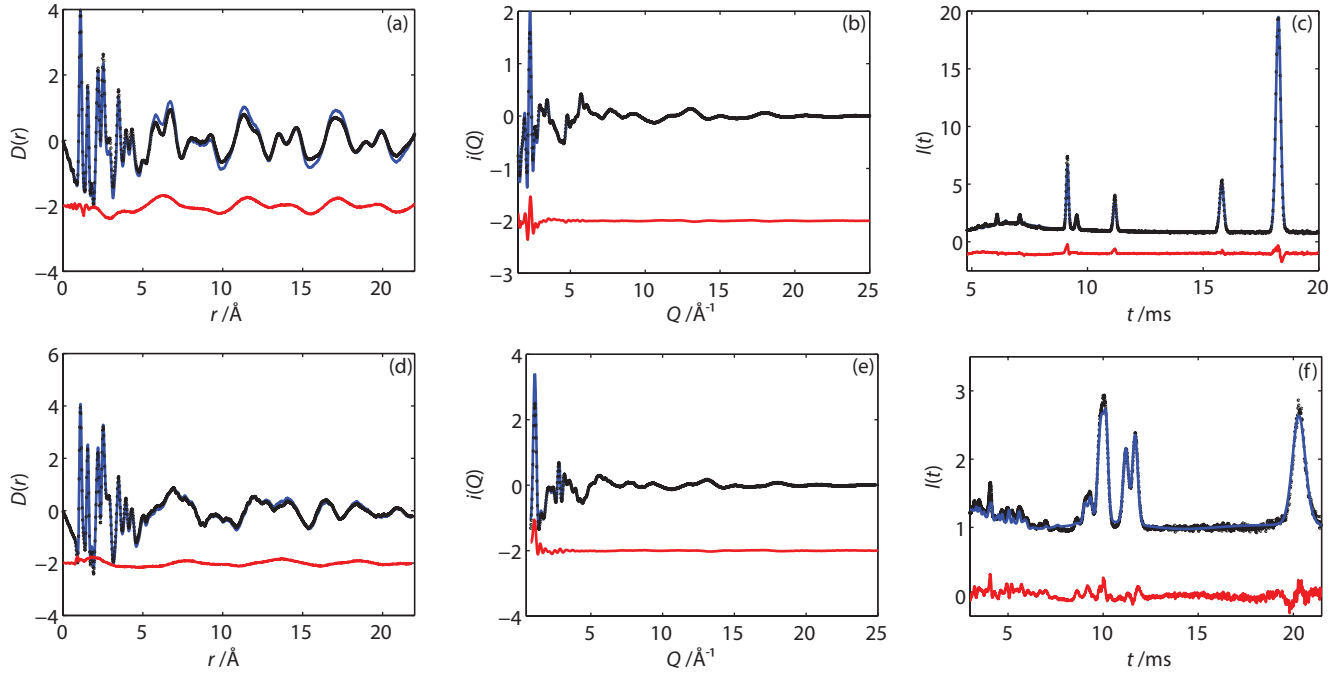

Figure 4: Converged fits to the pair distribution functions, scattering functions, and Bragg profiles of the disordered phases of adamantane (218 K; a–c) and adamantanecarboxylic acid (270 K; d–f). Experimental data are shown as black points, fit as a blue line, and residual as a red line.

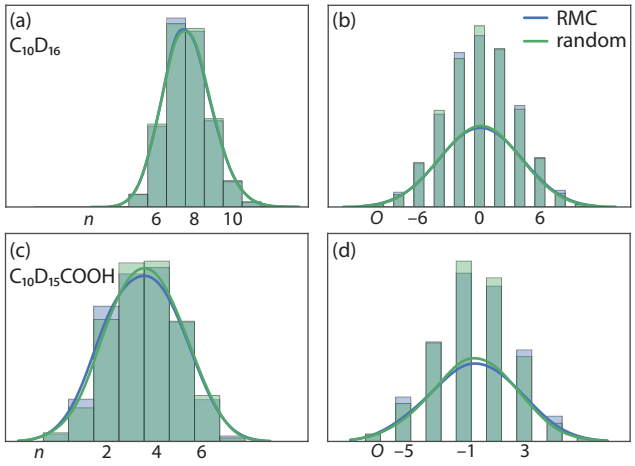

Figure 5: Histograms (blue) of the two ordering metrics, together with kernel density estimates as a guide to the eye, for adamantane at 218 K: (a) n and (b) O; and adamantanecarboxylic acid at 270 K: (c) n and (d) O. Also shown (green) are the same metrics for the random starting distribution projected onto the two predominant orientations for each material.

neighbours of a molecule i and $s = \pm 1$ represents the two orientations. This is a less precise metric since the correct value of O (-4 for adamantane; $+1$ for adamantanecarboxylic acid) is necessary but not sufficient for perfect order.

Representative histograms showing the distribution of each of these parameters in the initial and refined configurations are shown in Figure 5. At a temperature of 10 K above the phase transition, neither distribution in either material differed significantly from the random initial orientations. This absence of local correlations, even immediately above the phase transitions, demonstrates that both transitions are strongly first order. This is expected both from symmetry analysis (for a phase transition involving two coupled order parameters and an isosymmetric phase transition respectively) and from sharp peaks in differential scanning calorimetry data,[7,8] but has not previously been directly observed. First-order behaviour is common to most monosubstituted adamantane derivatives, with the exception of 1-adamantylmethanol, in which the high-temperature disorder involves the substituent rather than the adamantyl groups.[12]

This analysis furthermore confirms the published crystal structure of the high-temperature phases. In particular, the literature determination of the high-temperature structure of adamantane relies on a detailed analysis of the calculated phase angle in the hypothetical non-centrosymmetric $F\bar{4}3m$ model to establish that the structure is centrosymmetric.[34] By contrast, RMC simulation was able, starting from a completely random distribution of orientations and exploring

the parameter space of all possible orientations, to reproduce the proposed crystal structure. It is remarkable, and testament to the strength of the van der Waals forces stabilising the allowed orientations, that, despite the plasticity of the high-temperature phases, few molecules are found between these orientations. Since RMC naturally tends to *introduce* randomness into atomic configurations, that it produced a more ordered structure than the initial configuration is strong evidence for this bimodal distribution of orientations. Combining these conclusions gives a picture of the intermolecular interactions in these materials in which the potential energy of a given molecule depends strongly on its own orientation, so that it spends most time in one of the two allowed orientations and little time between them, but only very weakly on the orientation of neighbouring molecules, producing little correlation between neighbours.

Finally, from the perspective of method development, these results demonstrate convincingly that RMC methods where each step moves a single atom are able to rotate large molecules with the assistance of appropriate interatomic potentials; introducing a more complicated step, such as directly rotating some molecule by a random angle or switching between RMC and MD simulation[30] was not necessary. The correlated atomic motion between starting and refined configurations, however, explains the relatively high number of RMC moves required before the high-temperature refinements reached equilibrium. RMC methods are thus a useful way to explore correlations associated with phase transitions in crystalline molecular solids, even where each molecule contains many atoms.

We are pleased to acknowledge the ISIS Neutron and Muon source for neutron beam time and the EPSRC for provision of the MidPlus high-performance computing system on which the calculations were performed (EP/K000233/1, EP/K000128/1), and for a studentship for E. O. R. B.

References

[1] H. Schwertfeger, A. A. Fokin, P. R. Schreiner, *Angew. Chem. Int. Ed.* **2008**, *47*, 1022–1036.

[2] N. D. Drummond, A. J. Williamson, R. J. Needs, G. Galli, *Phys. Rev. Lett.* **2005**, *95*, 096801.

[3] S. Roth, D. Leuenberger, J. Osterwalder, J. E. Dahl, R. M. K. Carlson, B. A. Tkachenko, A. A. Fokin, P. R. Schreiner, M. Hengsberger, *Chem. Phys. Lett.* **2010**, *495*, 102–108.

[4] C. F. Matta, J. Hernández-Trujillo, T.-H. Tang, R. F. W. Bader, *Chem. Eur. J.* **2003**, *9*, 1940–1951.

[5] P. R. Schreiner, L. V. Chernish, P. A. Gunchenko, E. Y. Tikhonchuk, H. Hausmann, M. Serafin, S. Schlecht, J. E. P. Dahl, R. M. K. Carlson, A. A. Fokin, *Nature* **2011**, *477*, 308–311.

[6] M. Zhang, C. F. Zukoski, *Langmuir* **2014**, *30*, 7540–7546.

[7] S.-S. Chang, E. F. Westrum, Jr., *J. Phys. Chem.* **1960**, *64*, 1547–1551.

[8] P. D. Harvey, D. F. R. Gilson, I. S. Butler, *J. Phys. Chem.* **1986**, *90*, 136–139.

[9] T. Clark, T. M. O. Knox, H. Mackle, M. A. McKervey, *J. Chem. Soc. Faraday Trans.* **1977**, *73*, 1224–1231.

[10] R. M. Paroli, N. T. Kawai, I. S. Butler, D. F. R. Gilson, *Can. J. Chem.* **1988**, *66*, 1973–1978.

[11] P. Negrier, M. Barrio, J. L. Tamarit, D. Mondieig, *J. Phys. Chem. B* **2014**, *118*, 9595–9603.

[12] B. B. Hassine, P. Negrier, M. Barrio, D. Mondieig, S. Massip, J. L. Tamarit, *Cryst. Growth Des.* **2015**, *15*, 4149–4155.

[13] T. Clark, M. A. McKervey, H. Mackle, J. J. Rooney, **1974**, *70*, 1279–1291.

[14] R. C. Fort, P. v. R. Schleyer, *Chem. Rev.* **1964**, *64*, 277–300.

[15] J. Donohue, S. H. Goodman, *Acta Cryst.* **1967**, *22*, 353–354.

[16] S. M. Breitling, A. D. Jones, R. H. Boyd, *J. Chem. Phys.* **1971**, *54*, 3959.

[17] T. Ixo, *Acta. Crystallogr. B* **1973**, *29*, 364.

[18] V. Vijayakumar, A. B. Garg, B. K. Godwal, S. K. Sikka, *Chem. Phys. Lett.* **2000**, *330*, 275–280.

[19] V. Vijayakumar, A. B. Garg, B. K. Godwal, S. K. Sikka, *J. Phys. Condens. Matter* **2001**, *13*, 1961–1972.

[20] J. P. Amoureux, M. Bee, J. Virlet, *Mol. Phys.* **1980**, *41*, 313–324.

[21] M. Bee, J. P. Amoureux, R. E. Lechner, *Mol. Phys.* **1980**, *40*, 617–641.

[22] K. Rapcewicz, J. Przystawa, *Physica B* **1995**, *205*, 115–120.

[23] H. T. Stokes, D. M. Hatch, *J. Appl. Cryst.* **2002**, *35*, 379.

[24] G. Subías, E. Palacios, J. Blasco, J. García-Ruiz, *J. Phys.: Condens. Matt.* **1996**, *8*, 8971.

[25] F. Bélanger-Gariépy, F. Brisse, P. D. Harvey, D. F. R. Gilson, I. S. Butler, *Can. J. Chem.* **1990**, *68*, 1163–1169.

[26] A. K. Soper, GudrunN and GudrunX: Programs for correcting raw neutron and X-ray diffraction data to differential scattering cross section, Technical Report RAL-TR-2011-013, Rutherford Appleton Laboratory, Didcot, U.K., **2011**.

[27] B. H. Toby, *J. Appl. Cryst.* **2001**, *34*, 210–213.

[28] A. C. Larson, R. B. V. Dreele, General Structure Analysis System (GSAS), Technical Report 86-748, Los Alamos National Laboratory, NM, U.S.A., **1994**.

[29] M. G. Tucker, D. A. Keen, M. T. Dove, A. L. Goodwin, Q. Hui, *J. Phys.: Condens. Matt.* **2007**, *19*, 335218.

[30] O. Gereben, L. Pusztai, *J. Comput. Chem.* **2012**, *33*, 2285–2291.

[31] G. Opletal, T. Petersen, B. O'Malley, I. Snook, D. G. McCulloch, N. A. Marks, I. Yarovsky, *Mol. Simul.* **2002**, *28*, 927–938.

[32] N. L. Allinger, Y. H. Yuh, J. H. Lii, *J. Am. Chem. Soc.* **1989**, *111*, 8551–8566.

[33] D. W. Greig, G. S. Pawley, *Mol. Phys.* **1996**, *89*, 677–689.

[34] C. E. Nordman, D. L. Schmitkons, *Acta Cryst.* **1965**, *18*, 764–767.

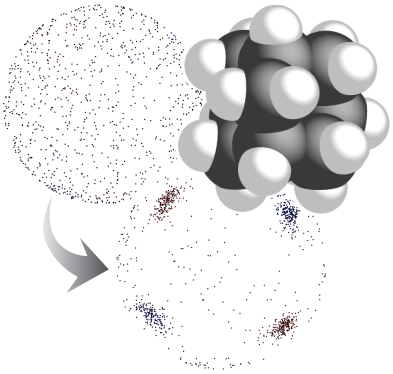

Short-sighted: Total neutron scattering data reveal no correlation between the orientations of neighbouring molecules in the disordered phases of adamantane or adamantanecarboxylic acid. Despite the high molecular symmetry, reverse Monte Carlo refinement from initially random molecular orientations shows that these orientations in both materials follow a strongly bimodal distribution (shown for adamantane in figure).